The Journal of Chemical Physics

RESEARCH ARTICLE | JANUARY 05 2024

A story of two transitions: From adhesive to abrasive wear and from ductile to brittle regime

Special Collection: Adhesion and Friction

S. Z. Wattel ; J.-F. Molinari

J. Chem. Phys. 160, 014711 (2024)
https://doi.org/10.1063/5.0176553

The Journal of Chemical Physics ARTICLE pubs.aip.org/aip/jcp

A story of two transitions: From adhesive to abrasive wear and from ductile to brittle regime

Cite as: J. Chem. Phys. 160, 014711 (2024); doi: 10.1063/5.0176553
Submitted: 14 September 2023 • Accepted: 14 November 2023 •
Published Online: 5 January 2024

S. Z. Wattel[a] and J.-F. Molinari

AFFILIATIONS

Civil Engineering Institute, Materials Science and Engineering Institute, Ecole Polytechnique Fédérale de Lausanne (EPFL), Lausanne, Switzerland

Note: This paper is part of the JCP Special Topic on Adhesion and Friction.
[a]**Author to whom correspondence should be addressed:** sacha.wattel@epfl.ch

ABSTRACT

Atomistic simulations performed with a family of model potential with tunable hardness have proven to be a great tool for advancing the understanding of wear processes at the asperity level. They have been instrumental in finding a critical length scale, which governs the ductile to brittle transition in adhesive wear, and further helped in the understanding of the relation between tangential work and wear rate or how self-affine surfaces emerge in three-body wear. However, so far, the studies were mostly limited to adhesive wear processes where the two surfaces in contact are composed of the same material. Here, we propose to study the transition from adhesive to abrasive wear by introducing a contrast of hardness between the contacting surfaces. Two wear processes emerge: one by gradual accretion of the third body by detachment of chips from both surfaces and the other being a more erratic mixed process involving large deformation of the third body and removal of large pieces from the soft surface. The critical length scale was found to be a good predictor of the ductile to brittle transition between both processes. Furthermore, the wear coefficients and wear ratios of soft and hard surfaces were found to be consistent with experimental observations. The wear particle is composed of many concentric layers, an onion-like structure, resulting from the gradual accretion of matter from both surfaces. The distribution of sizes of these layers was studied, and it appears that the cumulative distribution of hard surface's chip sizes follows a power law.

I. INTRODUCTION

Wear is the damaging and gradual removal of material on surfaces. The study of wear is of utmost economical and environmental importance as the replacement of worn-out parts is estimated to represent an annual expenditure of 680×10^9 euros and to require 3% of the global energy expenditure to manufacture.[1] Two types of mechanical wear—wear originating of sliding contact between two surfaces—represent more than 80% of total wear across the world: (a) adhesive wear (when significant adhesive forces exist between surfaces of similar properties) and (b) abrasive wear (when there is a significant contrast of hardness between the surfaces).

Wear mechanisms live at the intersection of many research fields, such as solid and fluid mechanics, material science, and chemistry. This renders the comprehension of wear phenomena from the first principle arduous. One of the first physics-based wear laws is Archard's wear law,[2] which states that the wear volume V_w is proportional to the sliding distance s and the normal load P and inversely proportional to the hardness H,

$$V_w = k\frac{sP}{H}. \tag{1}$$

In the original formulation for adhesive wear, the dimensionless wear constant k has a physical meaning: it is related to the probability that matter detaches when two asperities collide. The magnitude of k varies from 10^{-8} to 10^{-1} and has to be measured empirically.[3] This wide range reduces its predictive power. Archard's wear law is also used for abrasive wear, taking H to be the hardness of the soft

surface,[3] even though the physical meaning of k is lost as abrasive wear does not originate only in particle detachment but also from scratching and cutting of the soft surface by the hard one.

Tribological research has been dominated by phenomenological studies looking for general trends or specific empirical laws, which can be useful for engineering design but lacks a foundation in physics. This culminated in the famed review publication of Meng and Ludema[4] compiling around 182 equations of wear, and more than a 100 parameters, of which none have better generalization capabilities than Archard's law.

A new generation of tribological research has recently emerged, thanks to the increasing power of computational mechanics. Indeed, during an experiment, observing "live" what happens between two surfaces as they slide against each other can be difficult. Numerical simulations offer a glimpse of the micromechanical world we cannot yet observe.

Atomistic simulations have been a cornerstone in the finding of a critical length scale d^*, which governs the transition, in adhesive wear,[5] from plasticity-dominated smoothing behavior to fracture-led, third-body creating behavior. This quantity was first discussed by Rabinowicz[3] in the context of asperity detachment but not applied to the ductile to brittle transition. The argument is that a particle detaches when the stored elastic energy becomes greater than the energy necessary to create a crack around the particle. The resulting length scale is proportional to the surface energy γ and the shear modulus G and inversely proportional to the square of the shear strength τ,

$$d^* = \lambda \frac{2\gamma_{surf} G}{\tau_{el}^2}, \tag{2}$$

With λ being a geometrical factor of the order of unity.

The family of interatomic pair potentials used to uncover d^* had a tunable hardness, which allowed, for the first time, to capture both ductile and brittle adhesive wear behaviors in a single model. By using potentials of the same family, work has been done to explore how applicable are Archard's assumptions at the asperity level,[6] the importance of frictional work to predict wear,[7] and how the critical length scale relates to Reye's theory of wear rate,[8] to the adhesive wear behavior of heterogeneous materials,[9] or to the ductile to brittle transition in cutting.[10] In this work, we propose to study the transition from adhesive to abrasive wear by introducing a contrast of hardness between the two contacting surfaces.

II. METHODS

All simulations are run using the MD software Large-scale Atomic/Molecular Massively Parallel Simulator (LAMMPS)[11] and are constrained to be two-dimensional in space. The parameters of the potentials used are detailed in Table I. Unless otherwise mentioned, all units are rendered dimensionless (reduced units) by taking a reference energy ϵ_0, length r_0 (respectively the depth and distance of the potential well), and atomic mass m_0 as well as a unity Boltzmann constant $k_B = 1$. The resulting reductions are summarized in Table II.

A. Tunable model potentials

The atomistic simulations use interatomic pair potentials for which short-range and long-range interactions are decoupled and can be tuned individually.[12] This is done by modifying the tail part of the potential without changing the part close to the energy well. Mechanically, this results in the possibility of changing the plastic properties (strength, hardness, etc.) without affecting the elastic ones (stiffness, equilibrium lattice spacing, surface energy, etc.). In doing so, brittle, fracture-dominated behavior can be favored at computationally-affordable scales.[5,6,12]

TABLE I. Potential parameters used for the simulations. The indices 0–9 correspond to the combination parameter f used to compute this potential, following Eq. (4). Shear strengths reproduced with permission from Wattel *et al.*, Extreme Mech. Lett. **57**, 101913 (2022). Copyright 2022 Elsevier B.V.[9]

Potential	P_0	P_1	P_3	P_5	P_7	P_9
F	0.0	0.1	0.3	0.5	0.7	0.9
τ	2.59	2.32	1.87	1.52	1.22	0.92
H	13.5	12.0	9.70	7.90	6.32	4.79
d^*	5.94	7.46	11.5	17.3	27.0	47.1

TABLE II. Table of reductions used to render all quantities dimensionless. These reductions are common within the atomistic simulation community and are sometimes referred to as Lennard–Jones reduced unit. k_B is the Boltzmann constant.

Quantity	Reduction
Distance	r_0
Mass	m_0
Energy	ϵ_0
Time	$r_0\sqrt{m_0\epsilon_0^{-1}}$
Velocity	$\sqrt{m_0^{-1}\epsilon_0}$
Force	$\epsilon_0 r_0^{-1}$
Pressure	$\epsilon_0 r_0^{-3}$
Temperature	$\epsilon_0 k_B^{-1}$
Shear rate	$r_0^{-1}\sqrt{m_0^{-1}\epsilon_0}$

The potential energy can be expressed as

$$\frac{V(r)}{\epsilon_0} = \begin{cases} \left(1 - e^{\alpha(r-r_0)}\right)^2 - 1, & r < 1.1r_0, \\ c_1\dfrac{r^3}{6} + c_2\dfrac{r^2}{2} + c_3 r + c_4, & 1.1r_0 \le r \le r_{cut}, \\ 0, & r_{cut} \le r, \end{cases} \tag{3}$$

where r is the interatomic distance, ϵ_0 is the depth of the well, r_0 is the interatomic distance of the bottom of the well, and $\alpha = 3.93\, r_0^{-1}$ is a parameter that tunes the stiffness. The tail of the potential can be shortened or elongated with r_{cut}. The parameters c_1, c_2, c_3, and c_4 are chosen to ensure continuity of the potential and its derivative at $r = 1.1r_0$ and $r = r_{cut}$.

In this work, the family of potentials used P_f results from a linear combination of three such potentials, P_b, P_m, and P_d,

$$P_f = (1-f)^2 P_b + 2f(1-f)P_m + f^2 P_d, \tag{4}$$

with the combination parameter f going from zero to one.

These combination potentials are used as they have an almost linear variation of shear strength, and thus hardness, with the

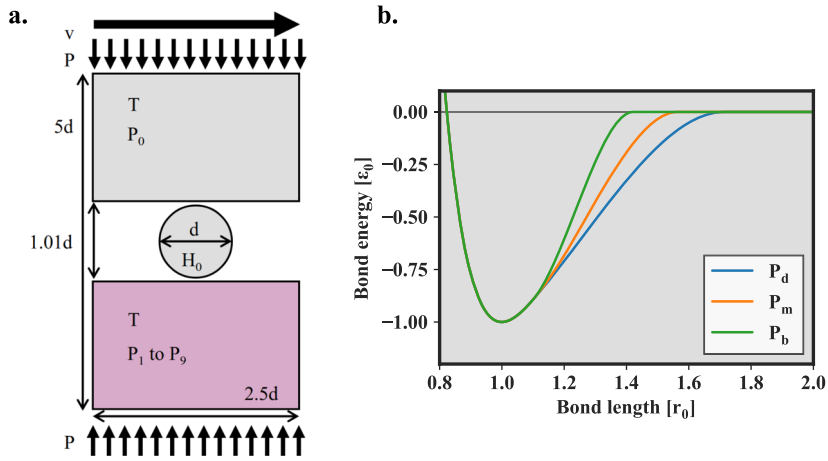

FIG. 1. (a) The simulation domain. The top surface and initial wear particle are hard (potential P_0), and the bottom surface is softer with potential varying from P_1 to P_9. All dimensions are scaled with the initial particle size d. (b) The three base potentials P_b, P_m, and P_d from which any potential P_f used in this work are a linear combination, following Eq. (4).

combination parameter.[9] The characteristics of the three base pair potentials, plotted in Fig. 1, are

- a short-tailed brittle one, P_b ($r_{cut} = 1.42r_0$),
- a long-tailed ductile one, P_d ($r_{cut} = 1.71r_0$),
- and an intermediate one, P_m ($r_{cut} = 1.56r_0$).

The boundaries of r_{cut} were chosen so that the transition from ductile to brittle behavior happens at a computationally affordable scale: the potential P_b starts to exhibit brittle behaviors at the scale of a few atoms, while P_d remains ductile until the scale of a 100 atoms.

B. Hardness measurements

Hardness is often defined as the indentation resistance of a material. However, atomistic simulations of indentation test at the scale of a few tens of atoms is unreliable as many parameters, such as the precise shape of the indenter or its movement relative to the orientation lattice, can result in a factor 10 difference in the measurement. Thus, the hardness is estimated from the shear strength τ with the following relation:[13] $H = 3\sqrt{3}\tau$. While the measurement of shear strength is also dependent on the exact method, we believe that it is more reproducible. The details and justification for the method of shear strength measurement can be found in Wattel *et al.*,[9] and relevant results for the current study are reproduced in Table I.

C. Three-body wear simulation

The simulation domain is initially composed of two surfaces and a circular third body. The diameter of the third body is varied between $d = 10r_0$ and $d = 100r_0$, and the domain is scaled accordingly as depicted in Fig. 1. The potential used for the top surface and the initial third body is the hardest one, P_0, whereas the potential for the bottom surface is varied between P_1 and P_9, all softer than P_0. Interactions between the soft surface and the hard component are ruled by the softer potential. A normal pressure P is applied on the top and bottom boundary. Four values of the pressure P are used: 0.01, 0.04, 0.07, and 0.1 (rendered dimensionless by the reductions detailed in Table II). The highest pressure is close to the one necessary to crush the third body when the softest potential P_9 is used. Initially, the third body is not in contact with the two surfaces, but the pressure puts them in contact. After a time $t = 2000$, the bottom boundary is fixed horizontally and the top boundary is submitted to a horizontal velocity $v = 0.15$. The simulations were run until a sliding distance $s = 500d$ was reached or for 12 h of computation time, whichever came sooner. All simulations reached at least a total sliding distance of $s = 250d$. The left and right boundary conditions are periodic. Initial velocities are distributed at random and scaled so that the initial temperature is 0.1, which equilibrates quickly to $T = 0.05$. The atoms are arranged in a hexagonal lattice, with an initial spacing corresponding to the equilibrium one at a temperature of $T = 0.05$. A six-atom-thick bulk-velocity-corrected Langevin thermostat[14] is present on the top and bottom, set at $T = 0.05$. The time-integration is done through a Verlet algorithm with a timestep of 0.005.

III. RESULTS

A. Wear behavior

Depending on the initial size of the wear particle and the hardness of the surfaces, two main behaviors could be identified. For larger size and harder materials, the wear particle rolls smoothly between the two surfaces and gradually detaches chips from both the soft and hard surfaces. The chips tend to be larger for the softer material. Even though material is also transferred back from the wear particle to the surface, the wear particle size still increases with time. The gradual removal of chips from both surfaces results in an onion-like structure of the wear particle, such as is shown in the middle snapshot of Fig. 2 and further discussed later.

The second behavior is observed for the wear particle of smaller initial size and for softer surface. The wear particle tends to get stuck

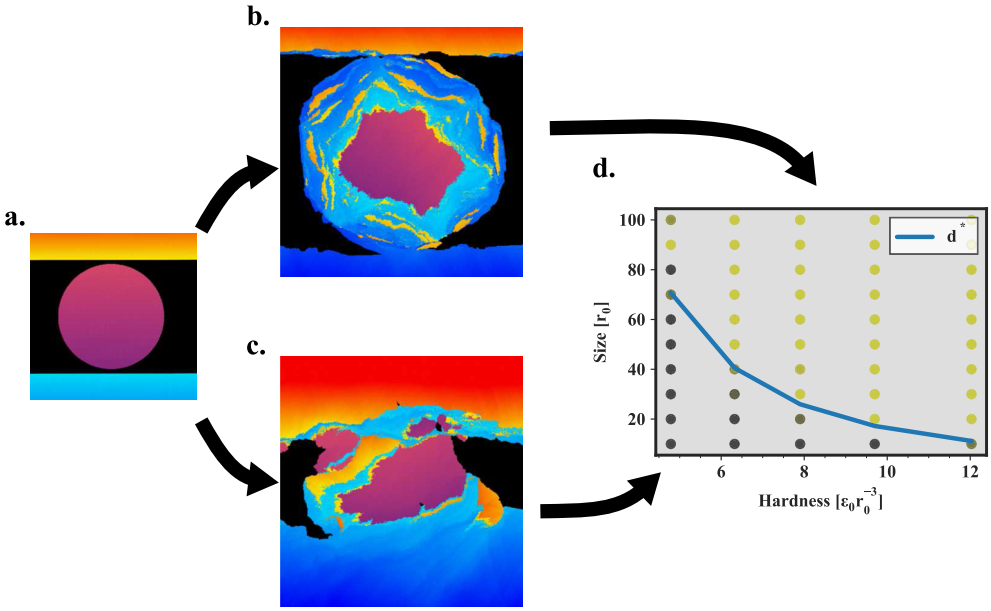

FIG. 2. (a)–(c) Snapshots of wear simulation for an initial particle diameter $d = 100$ atoms and $P = 0.1$. The whole simulation domain is not represented, and snapshots are a zoom. (a) Initial configuration: the colors help track the origin of atoms, and the color gradient highlights deformations. (b) End of the simulation for a soft surface of potential P_7 illustrating the gradual removal behavior. It is possible to visually isolate the orange chips coming from the hard surface. (c) For a soft surface of potential P_9. Here, the ductile behavior is clearly visible from the large deformation of the bottom soft surface and the hard third body. (d) Map of wear behaviors depending on hardness of the soft surface and initial size of the third body: yellow represents gradual removal, and black represents ductile behavior. The curve is the value of d^* with a pre-factor of $\lambda = 1.5$.

in the softer surface, removes large pieces of the softer material that may be larger than the particle, and/or breaks in several pieces and re-agglomerates. The snapshot (b) of Fig. 2 illustrates this behavior. The wear rate appears to be greater than in the first mode. However, as the deformations involved are large, they tend to reach the boundary conditions early in the simulation, after which the results are meaningless. This renders a quantitative analysis of the wear rate difficult. A surprising observation is that a softer surface actually leads to greater deformation in the hard initial third body, which goes against the initial intuition. One possible explanation is that the hard particle gets embedded more in the soft material, which prevents it from rolling and thus leads to plastic shearing-based behavior.

In Fig. 2, a map of the two behaviors is plotted. The axes are the initial particle diameter and the hardness of the soft surface. Each point represents four simulations at varying pressure. The gradient from yellow to black indicate whether most of the simulations showcased the first, gradual wear behavior or the second one, respectively. The results were discriminated by judging simulations snapshots by eye. Also plotted is the critical length scale d^* of the soft surface, which appears to be a good delimiter of both domains.

B. Third body structure resulting from the gradual wear behavior

Thereafter, unless otherwise mentioned, the results' analysis will be restrained to simulations showcasing the gradual wear behavior (more specifically, the 48 simulations with the softer surface potential P1 to P7, initial particle size 80–100 atoms). In this wear regime, the wear particle detaches chips from both surfaces and the resulting structure of the wear particle reflects this process. In Fig. 3, snapshots of the wear particle for surfaces with low contrast of hardness (a) and greater contrast of hardness (b) are shown. As chips are detached, they agglomerate concentrically around the particle. In the case of the higher contrast of hardness, as chips from the hard surface are significantly smaller than the one from the soft surface, they are easy to distinguish individually. For low contrast of hardness, the structure is more muddled. From these snapshots, it is possible to extract only the atoms that originally belonged to the hard surface [top right of Figs. 3(a) and 3(b)]. The chips of hard matter can be isolated by the following algorithm: first, a graph is created in which two atoms are connected if the distance (accounting for periodic boundary condition) separating them is less than a pre-defined cut-off, for us, $1.5r_0$. Then, atoms are considered to be part of the same cluster if there is a connected path between them. The resulting clustering is highlighted by the colors. The chips from the soft surface only form one or a few big clusters as they are mostly all connected; thus, no clustering analysis could be applied to them. These clusters are related to the original chips of matter removed from the surfaces by the accretion process but do not correspond to them one to one: a cluster might be composed of the amalgamation of several chips or an original chip could be sheared apart in several pieces. Indeed, the initial circular core of the wear particle loses its shape, and this is evidence that the particle undergoes significant deformation as it rolls.

Also present in Fig. 3 is a histogram of cluster sizes and a cumulative curve of cluster weight, both plotted on a double

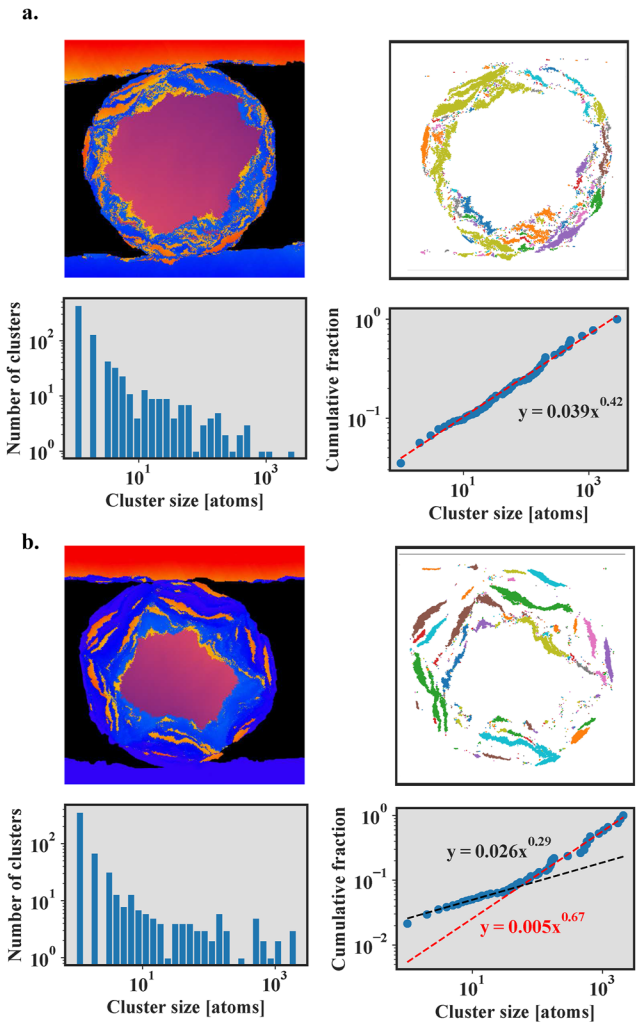

FIG. 3. Results from simulation with initial third body size of 100 atoms and a pressure of 0.04: (a) for a low contrast of hardness $H_0/H_3 = 1.4$ and (b) for a low contrast of hardness $H_0/H_7 = 2.1$. Top left: Simulation snapshot with the same initial coloring as in Fig. 2. Top right: Matter from the hard top surface, isolated and color-coded by cluster. Bottom left: Histogram of clusters by size. Bottom right: Normalized cumulative volume by cluster sizes, in logarithmic scale.

logarithmic scale. The second graph represents how much of the atoms belong to a cluster below a certain size. For simulation with a lower contrast (P_1 to P_5), the cumulative distribution appears to follow a power law. For the one with the highest contrast, the power law has two branches with different exponents: the large clusters represent a higher proportion of the total volume. One explanation could be that the higher quantity of soft matter aggregated quickly covers and protects the hard cluster. They get embedded in a soft matrix that prevents them being broken by or redeposited by the rolling motion. Thus, the higher proportion of large clusters might not be due to larger initial chips being removed but by preventing them being broken up.

C. Wear rate and volume

To estimate the wear volume at the end of the simulations, the wear particle was manually outlined. Then, atoms from the initial wear particle were removed, and the remaining atoms were counted. This count is considered to be the wear volume. To compare to Archard's wear law, the average wear rate measured at the end of the simulation is plotted against the constant normal force applied on the top and bottom boundaries. For all but the simulation with the softest potential P_9, the normalized worn volume is proportional to the pressure, in accordance with Archard's law, and the slopes of the linear regression give the wear coefficients. Different slopes are obtained for simulations with different soft surfaces. Even though the soft materials are very similar (same lattice, same elastic stiffness, for example), the only difference being the tail of the potential, Archard's law does not catch all the dependence of hardness on wear rate. In Fig. 4(b), the measured wear coefficients are plotted against the hardness, and a power law fit of exponent −1.9 is found. This is close to experimental results of wear rate with two surfaces of contrasting but relatively close hardness[3,15] where such power law scaling was also found with exponents between 2 and 6.

Archard's law breaks down for the simulations with the softest material. These simulations are at the edge of the ductile domain and starts displaying significant plastic shearing. As shearing is regulated by the tangential force, the dependence on the normal pressure reduces. This suggests that a law based on the tangential work instead of the normal pressure may be more relevant in this case or in general, as have been proposed before.[6]

Next, the wear of the hard and soft surface is studied independently. Even though one surface is harder, both get worn away during the sliding simulations. Knowing from which surface the wear is originating from can help predict the expected useful service life of an abrading tool for example. Experimentally,[3] the ratio between the worn volume from the soft surface and from the hard surface appears to follow a power law of the ratio of the hardness of both surfaces with an exponent between 2 and 3. The same ratios are plotted in logarithmic scales in plot (c) of Fig. 4, and a scaling of exponent of about 2.5 is also apparent. However, we do not wish to draw significant conclusion on the existence of a power law because of the large scatter in the data and the small range of hardness contrast, less than one order of magnitude, in the simulations. As of now, to the best of our knowledge, no fist-principle explanation has been provided for this scaling, and data, both experimental and numerical, are scarce. Finally, an interesting result is that the wear of the hard surface is not only weakly dependent on the hardness of the soft surface but is also counterintuitively slightly higher against softer surfaces. This is evidenced by plot (d) of Fig. 4, which shows the pressure-corrected volume worn from the hard surface for the different hardness contrasts. These results suggest that an abrading tool would be worn away at a similar rate irrespective of the tooled material hardness but would cut softer material faster, meaning that wear of the cutting tool would be better predicted by operating time rather than the amount of material cut away.

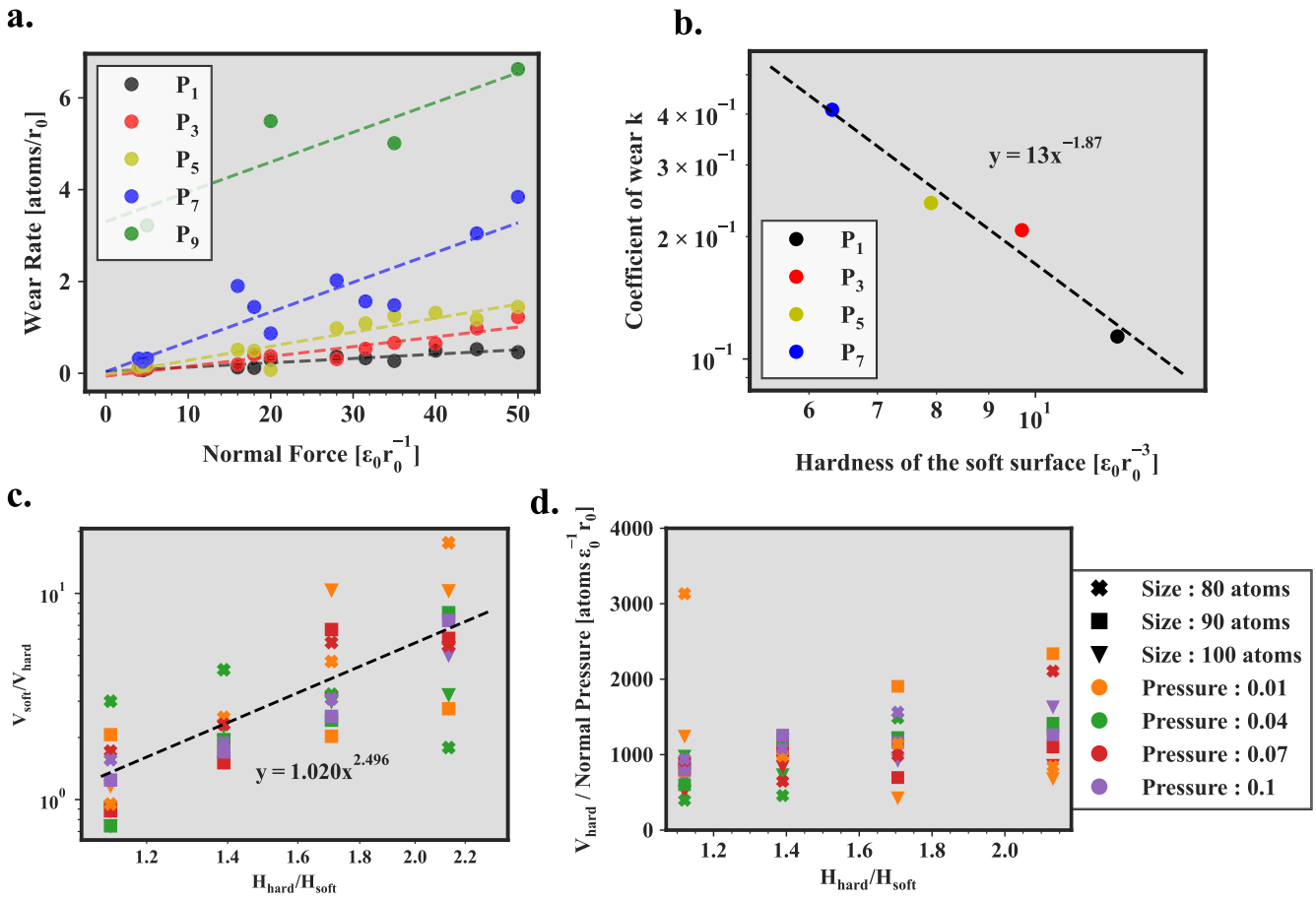

FIG. 4. (a) Wear rate plotted against normal force. The dashed curves are fitted linear regression. (b) Measured coefficients of wear [slopes of the dashed curves in (a) multiplied by hardness] against the hardness of the soft surface. (c) Ratio of volume worn away from each surface against ratio of hardness. (d) Volume worn away from the hard surface, divided by pressure, against the ratio of hardness.

IV. DISCUSSION

The tunable model potentials used in this work are not meant to represent any specific material but rather to allow the exploration of different mechanisms by varying a single parameter regulating ductility properties. However, they have been useful in further understanding the underlying mechanisms of wear and related process.[5,8,9] The model used in this work has been able to reproduce power scaling laws observed in experiments about wear rates and ratio of wear volume between hard and soft surfaces. This gives confidence that the model may be able to capture the mechanisms at the origin of these scaling laws.

The critical length scale was originally formulated to characterize asperity detachment in adhesive wear. Here, it has been found to govern another ductile to brittle transition. This suggests the existence of a characteristic length scale of general interest for ductile to brittle transition: the ratio of the Griffith critical energy release rate G_c to the maximum elastic strain energy density attainable $E_{el,\max}$,

$$d^* \propto \frac{G_c}{E_{el,\max}}. \tag{5}$$

Furthermore, for the removal of matter by cutting, a transition of ductile to brittle depending on the cutting depth is also ruled by a critical cutting depth l^*[16–18] depending on fracture toughness K_c and yield strength σ_y,

$$l^* = (K_c/\sigma_y)^2. \tag{6}$$

The fracture toughness can be expressed as $G_c \approx \frac{K_c^2}{E}$, with K_c being the fracture toughness and E being the Young modulus. By taking the maximum elastic strain energy density attainable to be approximately $E_{el,\max} \approx \sigma_y \epsilon_y \approx \frac{\sigma_y^2}{E}$, with ϵ_y being the strain at yield point, we obtain that d^* is proportional to l^*,

$$d^* \propto \frac{G_c}{E_{el,\max}} \propto \left(\frac{K_{1c}}{\sigma_y}\right)^2 = l^*. \tag{7}$$

For the wear of surfaces by gradual removal of matter by the third body, the surface is worn away chip by chip. Thus, the total worn volume is equal to the product of the average chip volume

$\bar{V}$, the frequency of chip removal f, and total sliding distance s. It could be qualitatively observed in the simulations that the chips tend to be thicker for softer surfaces. While the initial fracture angle of the chip depends on the size of the third body,[19] if we postulate, following these observations, that its thickness is proportional to d^*, then $\bar{V} \propto d^* \propto 1/H^2$, with H being the hardness. Assuming two surfaces of different hardness, the ratio of worn volume is $V_{soft}/V_{hard} \propto f_{soft}/f_{hard}\left(H_{hard}/H_{soft}\right)^2$. This provides a partial explanation of the power scaling between worn surface ratio and hard ratio. This hypothesis could be tested with further experiments and numerical simulations.

Finally, Archard's wear law, while formulated initially for adhesive wear, is often used for other types of wear, including abrasive wear. In recent years, a few studies have explored the application of Archard's wear law at the asperity-level. It was found that the frictional work was a better predictor of wear volume[6] than Archard's wear law. However, Archard's law could be recovered when the wear is plasticity-driven.[7] For fracture-driven wear as well as when the asperity size is much larger than the critical length scale d^*, the scaling of frictional work with wear was found to be sublinear.[7,8] As a direction of further study, it would be interesting to see how the results of these studies are applicable to abrasive wear at the asperity-level.

V. CONCLUSION

Simulations of three-body wear were run with surfaces of contrasting hardness. Two main behaviors could be isolated: one of gradual accretion of the wear particle by removal of chips from both surfaces and one displaying a more erratic behavior with a significant amount of plastic deformation and removal of pieces larger than the third body size. It was found that the critical length scale d^* was a good predictor of this ductile to brittle transition. For simulations displaying the behavior of gradual accretion, the wear coefficients as well as the ratio of matter worn from each surface follow power scaling laws found in experiments. Finally, these simulations allow us to look into the structure of the wear particle: the accumulation of chips create a concentric, onion-like structure. The chips originating from the hard surface could be isolated and their size is analyzed: the cumulative distribution of chip sizes also follows a power law, whose exponent depends on the hardness of the soft surface. However, the study was limited to a narrow range of hardness contrast due to the computational restriction, and we hope that this paper will spark interest in experimentalists to further investigate this relatively unexplored area of tribology.

ACKNOWLEDGMENTS

This work was supported by the Swiss National Science Foundation under the grant "Wear across scales" (Grant No. 197152).

AUTHOR DECLARATIONS

Conflict of Interest

The authors have no conflicts to disclose.

Author Contributions

S. Z. Wattel: Conceptualization (equal); Formal analysis (equal); Investigation (equal); Methodology (equal); Software (equal); Visualization (equal); Writing – original draft (equal); Writing – review & editing (equal). **J.-F. Molinari**: Conceptualization (equal); Funding acquisition (equal); Supervision (equal); Writing – review & editing (equal).

DATA AVAILABILITY

Input and post-processing files necessary to reproduce the results and plots presented here as well as a curated dataset are available at https://doi.org/10.5281/zenodo.10418500.

REFERENCES

[1] K. Holmberg and A. Erdemir, "Influence of tribology on global energy consumption, costs and emissions," Friction **5**, 263–284 (2017).
[2] J. F. Archard, "Contact and rubbing of flat surfaces," J. Appl. Phys. **24**, 981–988 (1953).
[3] E. Rabinowicz, *Friction and Wear of Materials* (Wiley, New York, 1995).
[4] H. C. Meng and K. C. Ludema, "Wear models and predictive equations: Their form and content," Wear **181-183**, 443–457 (1995).
[5] R. Aghababaei, D. H. Warner, and J.-F. Molinari, "Critical length scale controls adhesive wear mechanisms," Nat. Commun. **7**, 11816 (2016).
[6] R. Aghababaei, D. H. Warner, and J.-F. Molinari, "On the debris-level origins of adhesive wear," Proc. Natl. Acad. Sci. U. S. A. **114**, 7935 (2017).
[7] K. Zhao and R. Aghababaei, "Adhesive wear law at the single asperity level," J. Mech. Phys. Solids **143**, 104069 (2020).
[8] J. Garcia-Suarez, T. Brink, and J.-F. Molinari, "Breakdown of Reye's theory in nanoscale wear," J. Mech. Phys. Solids **173**, 105236 (2023).
[9] S. Wattel, J. Garcia-Suarez, and J.-F. Molinari, "Understanding the mechanisms of adhesive wear for heterogeneous materials through atomistic simulations," Extreme Mech. Lett. **57**, 101913 (2022).
[10] W. Zheng, L. Ma, S. Pei, and R. Aghababaei, "Numerical assessment of transition in cutting mode and its effect on roughness creation," Int. J. Mech. Sci. **261**, 108666 (2023).
[11] A. P. Thompson, H. M. Aktulga, R. Berger, D. S. Bolintineanu, W. M. Brown, P. S. Crozier, P. J. in't Veld, A. Kohlmeyer, S. G. Moore, T. D. Nguyen, R. Shan, M. J. Stevens, J. Tranchida, C. Trott, and S. J. Plimpton, "LAMMPS—A flexible simulation tool for particle-based materials modeling at the atomic, meso, and continuum scales," Comput. Phys. Commun. **271**, 108171 (2022).
[12] V. P. Rajan, D. H. Warner, and W. A. Curtin, "An interatomic pair potential with tunable intrinsic ductility," Modell. Simul. Mater. Sci. Eng. **24**, 025005 (2016).
[13] M. F. Ashby and D. R. H. Jones, *Engineering Materials 1: An Introduction to Properties, Applications and Design*, 4th ed. (Butterworth-Heinemann, Oxford, England, 2011).
[14] T. Schneider and E. Stoll, "Molecular-dynamics study of a three-dimensional one-component model for distortive phase transitions," Phys. Rev. B **17**, 1302–1322 (1978).
[15] E. Rabinowicz, "The wear of hard surfaces by soft abrasives," *Proceedings of the 1983 International Conference on Wear of Materials* (ASME, 1983), pp. 12–17.
[16] T. G. Bifano, T. A. Dow, and R. O. Scattergood, "Ductile-regime grinding: A new technology for machining brittle materials," J. Eng. Ind. **113**, 184–189 (1991).
[17] H. Huang, B. Lecampion, and E. Detournay, "Discrete element modeling of tool-rock interaction I: Rock cutting," Int. J. Numer. Anal. Methods Geomech. **37**, 1913–1929 (2012).
[18] R. Aghababaei, M. Malekan, and M. Budzik, "Cutting depth dictates the transition from continuous to segmented chip formation," Phys. Rev. Lett. **127**, 235502 (2021).
[19] E. Milanese and J.-F. Molinari, "A mechanistic model for the growth of cylindrical debris particles in the presence of adhesion," Int. J. Solids Struct. **203**, 1–16 (2020).